Photolithographic Fabrication of Upconversion Barcodes for Multiplexed Molecular Detection

Xiao Zeng, Sudheer Kumar Vanga, Eng Tuan Poh, Yi Shi, Chorng Haur Sow, Andrew Anthony Bettiol,* and Xiaogang Liu*

The demands of clinical diagnostics and genetic analysis for high-performance multiplex detection systems have driven substantial advancement from planar microarrays to suspension arrays for accurate encoding, inventorying, and detecting extensive databases of biomolecules. Despite the multitude of related works and the commercial availability of nanostructured arrays for biodetection, it remains challenging to develop biodetection modules of massive coding permutation with high production rates and fast reaction kinetics . Herein, the concurrent improvement in both production and coding capacities without compromising detection kinetics is reported using lithography-based upconversion barcodes as the basis for bioassay detection modules. This method exploits microstructural forms of dense graphical encoding, with barcode production up to 10^9 per run at extensive color permutations. The upconversion barcoding technique requires a million times lower analyte consumption compared to currently available technologies. Moreover, the use of upconversion barcodes is demonstrated in a DNA hybridization test with high target specificity, low detection limit, and ease of flexible surface bioconjugation, enabling potential development of biomarkers in the analysis of massive proteomics, genomics, and metabolomics data.

In proteomics and genomics research for clinical discovery, suspension array technology has enabled high-throughput molecular interaction screening and gene/protein expression profiling with minute analyte consumption.[1] For suspension-based assays, intermolecular binding and dissociation occur rapidly on the surface of microparticles suspended in buffer solutions. These molecular interactions can be subsequently quantified by a statistical conclusion from individual microparticle examinations across the whole ensemble using high-speed readout methods. Since multiple analytes have to be detected simultaneously in mixed suspensions containing tens of thousands of microparticles tagged with variable biomolecule probes, it is critical to encode each microparticle subpopulation prior to the mixing step so that the molecular status on particle surfaces can be successfully tracked throughout the assay.[2]

In principle, a single microparticle with large coding capacity offers high potential for multiplexed assay of molecular interactions. To expand encoding capacities, several microparticle-encoding methods have been developed. Among them, fluorescence encoding remains the most established method,[3] by which fluorophore mixes of predefined emission colors and concentration ratios are incorporated into microbeads to create an encoded library of ≈100 members.[3c,4] In theory, the total encoding capacity can be further expanded by recruiting a myriad of dye color database and by fine-tuning their concentration ratios. However, the associated smaller contrast in signal readout may lead to increased error rates due to challenges in deconvoluting similar spectral fingerprints across single particles.

In contrast, generating patterns on a microparticle brings additional graphical elements to the existing fluorescence encoding paradigm. The combination of spectral and graphical approach can potentially lead to a drastic expansion in the coding permutation.[5] A six segmented barcode with ten distinct colors arranged in a parallel array can afford up to one million (10^6) coding combinations.[6] Despite the remarkable coding capacity endowed with the color-graphical approach, the sophistication in the material architecture generally requires the barcodes to be produced one at a time, even with specialized instrumentation. The relatively low production rate and associated high cost impede the widespread of these colored barcodes. Additionally, the produced barcodes typically have dimensions three orders of magnitude larger than sub-10 μm

Dr. X. Zeng, Prof. X. Liu
Department of Chemistry
National University of Singapore
3 Science Drive 3, Singapore 117543, Singapore
E-mail: chmlx@nus.edu.sg

Dr. S. K. Vanga, Dr. Y. Shi, Prof. A. A. Bettiol
Centre for Ion Beam Applications
Department of Physics
National University of Singapore
2 Science Drive 3, Singapore 117542, Singapore
E-mail: a.bettiol@nus.edu.sg

E. T. Poh
Graduate School for Integrative Sciences and Engineering (NGS)
National University of Singapore
Singapore 117456, Singapore

Prof. C. H. Sow, Prof. A. A. Bettiol
Department of Physics
National University of Singapore
2 Science Drive 3, Singapore 117551, Singapore

The ORCID identification number(s) for the author(s) of this article can be found under https://doi.org/10.1002/adom.202001168.

DOI: 10.1002/adom.202001168

ADVANCED
SCIENCE NEWS

www.advancedsciencenews.com

ADVANCED
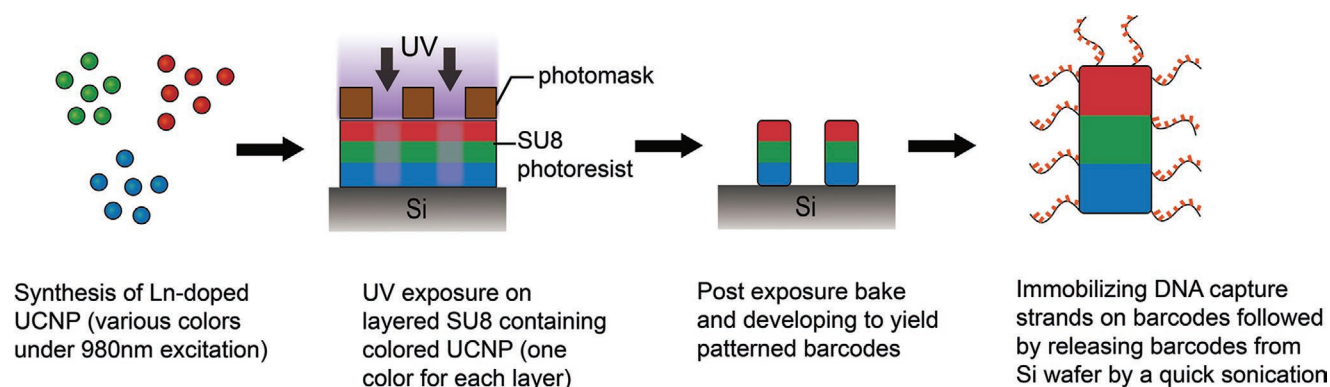OPTICAL
MATERIALS

www.advopticalmat.de

Figure 1. Schematic illustration of the fabrication process of DNA molecules immobilized microbarcodes. UCNPs with their characteristic emission colors are mixed with SU-8 and spin-coated repeatedly onto Si substrate to form multilayer thin films. The film subsequently undergoes UV exposure. The exposed regions would be cross-linked and remain unwashed during the developing stage. Biomolecules, including DNA and proteins can be covalently conjugated to the microbarcode surface thereafter and a brief sonication lifts all the molecule-tagged barcodes for further detection experiments.

microparticles used in traditional suspension assays. Consequently, the reduced surface-area-to-volume ratio prevents fast mixing kinetics, which is an essential trait in suspension assay technologies.

Herein we report a photolithography-based technique for mass production of miniaturized color-graphical barcodes. This newly developed method offers a production rate over ten thousand times faster than that achieved with state-of-the-art flow lithography techniques.[5f,7] As a result of miniaturization of encoded microparticles, the material consumption on each microparticle is calculated to be a million times lower than that required in previous attempts.[6] Meanwhile, the produced microbarcodes have an expected coding capacity of over ten thousand, comparable to mainstream DNA or protein microarrays. We also demonstrate that a myriad of various biomolecules, including DNA, RNA and proteins, can be conveniently linked to barcode surfaces in a one-step reaction. The obtained biomolecule-tagged microparticles are readily available for multiplexed molecular screening and detection in a suspension assay.

To construct multicolor graphical barcodes, luminescent materials of various emission colors were first mixed with a negative tone photoresist SU-8 (**Figure 1**). These particle-containing photoresists were spin-coated onto a silicon substrate in a layer-by-layer fashion according to a predetermined emission color sequence. Consequently, luminescent materials of contrasting colors can be spatially segregated in adjacent layers within a 15 µm thin film, providing the basis for barcode formation. The obtained multilayer film subsequently underwent a series of treatments, including UV exposure, postexposure baking, and developing, to afford a micropillar array on which biomolecules tagging can be performed. Finally, a brief sonication step liberates microparticles off the substrate and into the buffer solution, allowing for luminescence microscopy of color permutations within a given microparticle and decoding of surface-bound molecules.

Prior to the barcode fabrication process, it is crucial to select a suitable luminescent material for color encoding. Considering that molecular interactions on microparticle surfaces are typically quantified by fluorescence techniques, using similar fluorophores for internal optical encoding is likely to cause spectral crosstalk between the detection and decoding process.

For this reason, lanthanide-doped upconversion nanoparticles (UCNPs) capable of converting near-infrared (NIR) excitation into visible emission becomes an appropriate candidate as the color encoding foundation in this work.[8] Similar to other works involving UCNP emissions and decay lifetimes for multiplexed bioimaging and encoding,[9] our barcode readout under NIR excitation is expected to impose zero interference to the fluorescence detection which utilizes visible light excitation.[10] Apart from the anti-Stokes property, upconversion materials are also known for their flexible color output tunability under single-wavelength excitation.[11] In this study, we prepared UCNPs that emit three primary colors, namely red (R), green (G), and blue (B). Through ratiometric mixing of the RGB nanoparticles, a series of emission colors ranging from purple to red can be achieved for optical encoding (**Figure 2**; Table S1, Figures S1 and S2, Supporting Information).

In the initial trials to craft UCNPs in SU-8 spin-coat single layers, we discovered that the nanoparticle dispersibility within the photoresist matrix marks a critical factor toward successful barcode production. Considering that each fabricated barcode has a height of 15 µm, any particle aggregation as large as 10 µm would almost span over the entire micropillar, making it impossible to read the coded information. In addition, the random distribution of particle agglomeration would render nonuniformity in the multilayered film, resulting in high inconsistency even within a singular batch of barcodes. This inhomogeneity dramatically increases the error rates in the decoding process (Figure S3, Supporting Information). To address this issue, we envision that by switching the oleate surface ligands on UCNPs for benzoate ions, the mixing of the nanoparticles with the benzene-ring-rich SU-8 photoresist would be made more effective owing to favorable π-π stacking interactions. After the ligand exchange step, UCNPs can be homogenously distributed in the SU-8 film, as evidenced by uniform upconversion emission from micropillars in the array (Figure S3, Supporting Information). Meanwhile, transmission electron microscopy analysis corroborates that the nanoparticles are mostly monodispersed in the polymer matrix (**Figure 3**a).

At this stage, although as-developed micropillars consist of multiple colored layers, the luminescence microscopy only reveals the overall merged emission color of the standing array
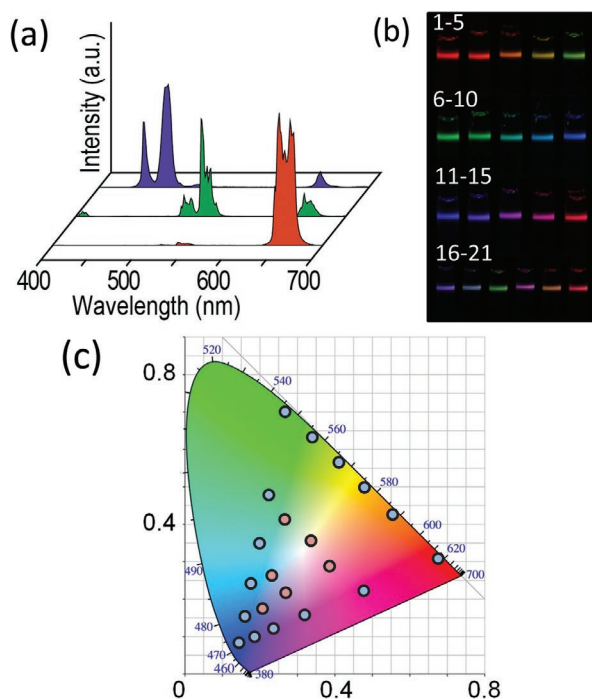
**ADVANCED
SCIENCE NEWS**

www.advancedsciencenews.com

**ADVANCED
OPTICAL
MATERIALS**

www.advopticalmat.de

Figure 2. a) Luminescence spectra of the UCNPs that emit the three primary colors (980 nm excitation). b) Luminescence images of the ratiometrically mixed UCNP solution. The first three rows are images obtained on dual-color mixing, and the last row represents tri-color mixing systems. (Solution composition and their upconversion luminescence spectral can be found under Table S1 and Figure S1, Supporting Information). c) The color gamut of the corresponding nanoparticle mixture. Outer triangle reflects the color coordinates from dual-color mixing system while the inner triangle indicates that for tri-color mixing.

of barcodes from a bird's eye perspective (Figure 3b–d). To characterize the color sequence, it is necessary to orient the barcodes such that sidewalls are exposed to the microscope objective. We found that a 30 s sonication step is sufficient to liberate all SU-8 structures off the silicon substrate. After drying the suspension on a glass substrate, micropillars with an aspect ratio of 3:1 would be naturally laid down due to a lowered center of gravity (Figure 3e). In comparison, structures with lower aspect ratios still own a great probability of orienting their upper surface to the objective lens, preventing proper barcode readout (Figure S4, Supporting Information). Although microstructures bearing an aspect ratio higher than seven can also be fabricated with smaller features, these micropillars tend to collapse during the development step due to the reduced adhesion of the narrower cross-section (Figure S5, Supporting Information). This unwanted barcode pre-lifting impedes subsequent biomolecule tagging and results in a decreased production yield. Therefore, for microbarcodes suspension assay in the following discussion, microstructures at an aspect ratio of 3:1 were utilized for the sake of smooth decoding.

In terms of color-graphical encoding, it is intuitive to correlate the increasing quantity of color layers inside the microstructure to higher encoding capacity. In an ideal scenario, if nanoparticle-photoresist mixtures can be spin-coated layer-by-layer indefinitely, the fabricated micropillars would carry an unlimited number of color permutations. In practice, however, the maximum coding number is heavily influenced by the film thickness progression and nanoparticle interlayer diffusion during the manufacturing process. In our spin-coating trials, we noticed that the total thickness of the prepared thin film scales in a nonlinear fashion upon repeated spin-coating. Instead, from the second layer onward, each new round of spin-coats
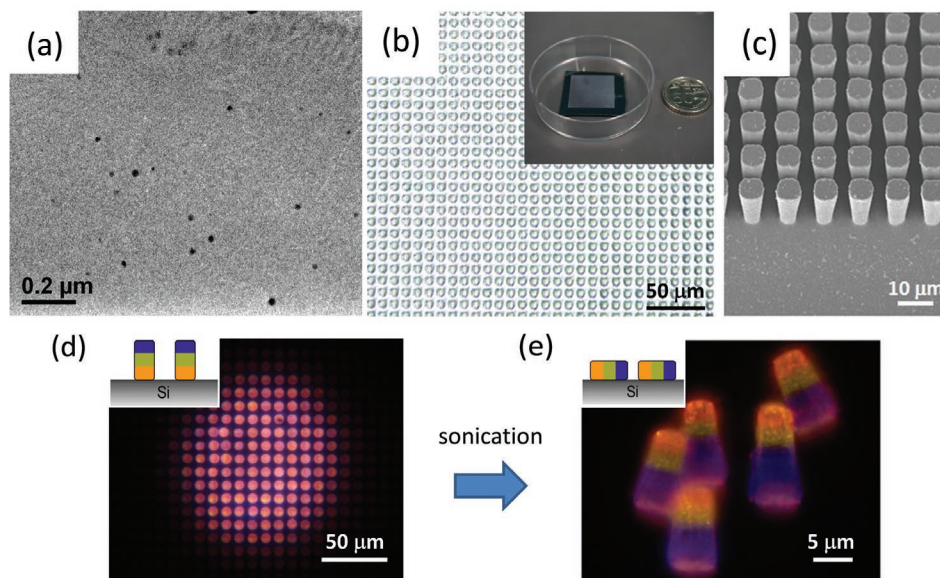

Figure 3. a) TEM image of the trimmed SU-8 film containing well-dispersed UCNPs. b) Optical microscopy image of the as-developed barcode array on Si substrate. Inset shows the size comparison between the patterned surface and a 50 cents coin. c) SEM image of the barcode array from an angled perspective. The base of the barcodes has a 4.5 µm diameter while the top dimension measures 5.5 µm. The average height of the barcodes is ≈12 µm. d) Luminescence microscopy of the barcode array from a top-view angle. A 980 nm excitation laser is focused onto the image center. Although the barcodes contain multiple layers, the top view does not allow sequence readout. e) Luminescence microscopy of the barcodes released from the Si substrate via sonication. The horizontally positioned barcodes permit easy color sequence readout for decoding purposes.
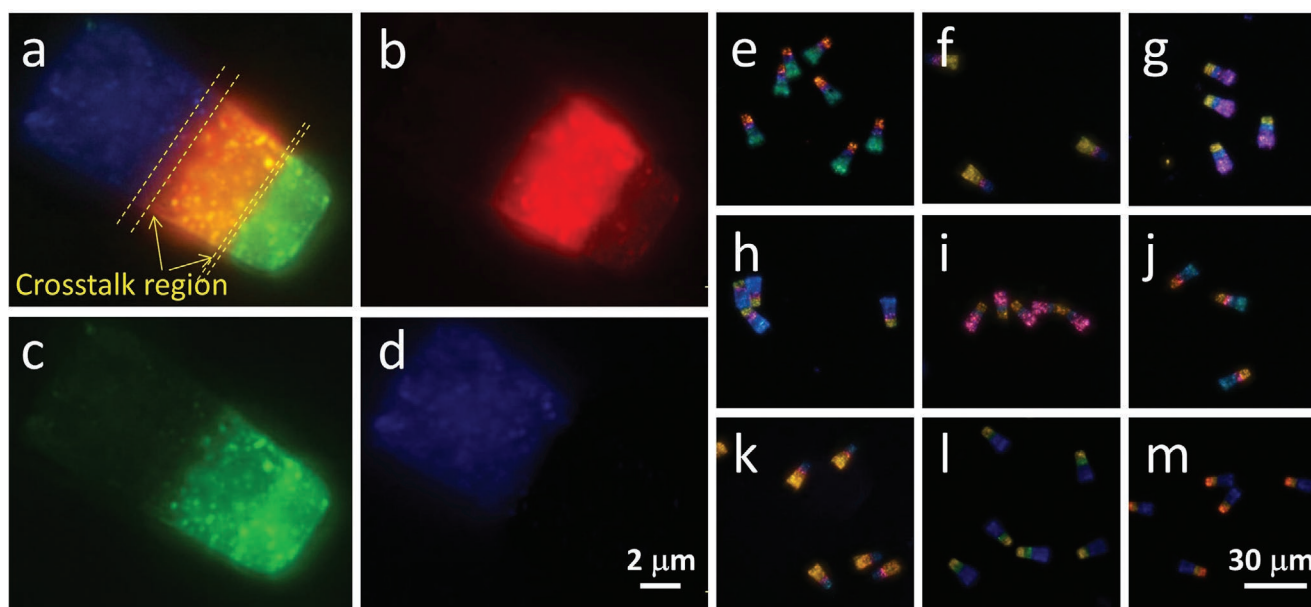
ADVANCED
SCIENCE NEWS
www.advancedsciencenews.com

ADVANCED
OPTICAL
MATERIALS
www.advopticalmat.de

Figure 4. a) High-magnification luminescence microscopy images of a single barcode with the color sequence of green–orange–blue (G–O–B). b–c) The same barcode viewed through red, green, and blue channels. The relatively sharp boundaries between neighboring layers indicate minimal nanoparticle interlayer diffusion during spin-coating fabrication. e–m) Luminescence microscopy images of additional barcodes with various color permutations captured under 980 nm wide-field illumination.

would only give rise to a small step increase in the overall film thickness (Figure S6c, Supporting Information). Luminescence microscopy further reveals that the thicknesses of individual color layers within the microstructure are dissimilar. The topmost layer is always the thickest, spanning almost half of the entire vertical dimension (Figure S6d, Supporting Information). Based on this thickness progression pattern, we believe that the pre-existing films tend to be compressed on subsequent spin-coating steps. When the process exceeds three rounds, this compression leads to a certain degree of color merging, creating ambiguity in the decoding outcome (Figure S6e,f, Supporting Information). On a three-layered microstructure, relatively sharp color contrast can be observed at layer boundaries, suggesting negligible interlayer-nanoparticle diffusion despite the sizeable centrifugal force during spin-coating (**Figure 4**a–d). In addition, given the asymmetrical color layout due to variations in layer thickness within these microbarcodes, R–G–B and B–G–R pairs in reverse order can now be differentiated.

From the discussion above, it can be estimated that if UCNPs of twenty distinguishable colors are incorporated into a three-layered microstructure, a total encoding capacity of 8000 (20^3) unique combinations can be achieved from these sub-15 µm particles. If downshifting luminescent materials such as quantum dots, can be further introduced into the layer permutation, the coding number could be expanded beyond a million by taking NIR and UV dual-channel excitations for barcode readouts. It should be noted that the real coding number is also affected by the instrumentation used. For instance, when UCNPs of similar color profiles are enrolled into a single microbarcode, the microscopic decoding becomes challenging using an ordinary microscope camera (Figure S7, Supporting Information). Advanced camera systems or spectrometers should thus be employed to decipher barcodes with similar colors.

Apart from a decent coding capacity, high-speed production of encoded microparticles is another desirable feature for suspension assay, considering that a typical biodetection trial consumes up to tens of thousands of microparticles. Since photolithography is a widely adopted technique for mass replication of microsized patterns, this newly reported method can produce large batches of color-barcodes at rapid rates without the need for additional specialized equipment. With a 6 inch wafer, 5×5 µm^2 micropillars with an interpillar spacing of 5 µm can be simultaneously produced at a rate close to 10^9 particles per photolithography process, which takes merely an hour to complete. In comparison to methods that prepare barcodes one at a time, the production rates generally do not exceed 10^5 h^{-1}.

The photolithography-based method not only offers a superior production rate but also reduces the amount of raw material (lanthanide precursors and SU-8) during barcode manufacturing. The microbarcodes produced in this work are 1700 times smaller than those prepared by stop-flow lithography reported previously.[6] The size miniaturization allows a significant reduction in material consumption. In addition, when decoding these small barcodes, objectives with high numerical aperture can be used to enable tight focusing of the laser beam. When the laser spot is reduced from 250 to 15 µm, the laser power density increases over a hundredfold, translating to an enhancement in emission intensity on the magnitude of five orders, owing to the nonlinear nature of the upconversion process. With such an enhancement, even if UCNPs are doped into SU-8 photoresist at a low mass concentration of 0.15%, sufficiently intense upconversion emission can be captured under high numerical aperture for fast and accurate decoding. As the use of high numerical aperture lens may limit the number of barcodes in the field of view, automated scanning microscopy can thus be considered as a possible implementation for future
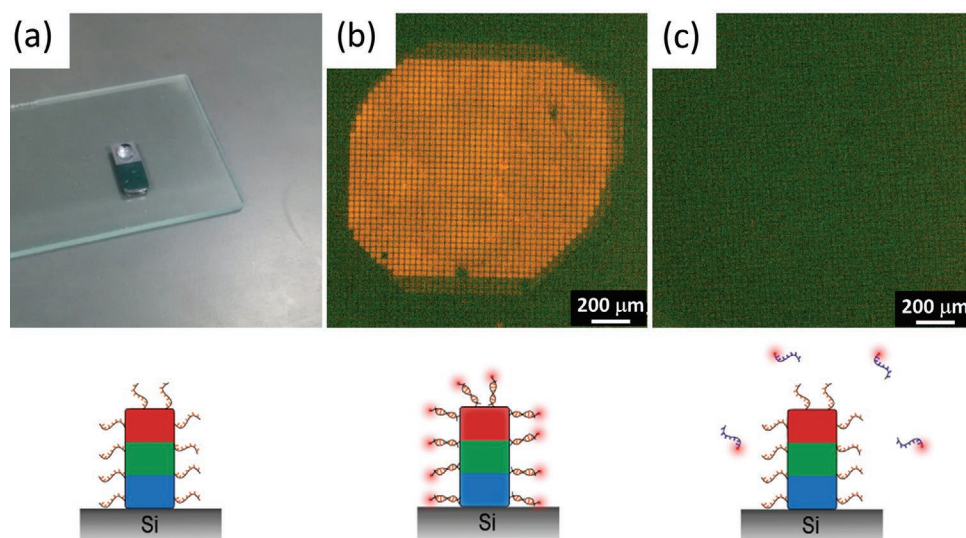
Figure 5. a) A photograph showing the reaction process of conjugating probe DNA strands onto the SU-8 surface. b) Hybridization trial on barcode array. After immobilizing the probe DNA strands onto SU-8, complementary DNA strands (Cy3 labeled) are transferred onto the SU-8 substrate. Hybridization takes place, as evidenced by the luminescence mark left on the SU-8 after stringent wash. In regions outside the luminescence circle where capture DNA strands do not exist, the weak fluorescence signal is detected, indicating that negligible nonspecific absorption occurs on SU-8 surfaces. c) When noncomplementary DNA (Cy3 labeled) is applied to the substrate, fluorescence is not detected, hence hybridization is not achieved.

high throughput decoding. In conclusion, owing to the reduced microparticle size and decreased nanoparticle doping concentration, the total consumption of lanthanide-doped UCNPs can be lowered to 7.5×10^{-10} mg per microparticle, a million times lower than existing methods.

For biomolecular recognition on the microbarcode surface, it is necessary to covalently tag the relevant probe molecules onto the barcodes before utilizing the suspension assay. Being an epoxy-based photoresist, SU-8 retains a significant amount of uncrosslinked epoxy groups on the material surface after the developing step. These epoxy functionalities allow for subsequent bioconjugation through nucleophilic ring-opening reactions.[12] To test the efficiency in biomolecular tagging on the microstructure surfaces, we incubated the as-developed SU-8 micropillars with amine-terminated single-strand DNA (ssDNA) prior to a hybridization test conducted directly while the barcode array is still on the silicon substrate. After Cy3 labeled ssDNA targets are applied to the micropillar array, the SU-8 pillars tagged with the complementary probe DNA strands exhibit strong orange fluorescence, indicating that hybridization has occurred effectively on the microstructure surface (**Figure 5**a,b). Meanwhile, in regions of negative control, where the probe ssDNAs are not tagged onto the SU-8 or noncomplementary to the Cy3 ssDNA targets, a negligible fluorescence signal was detected (Figure 5c). This result substantiates the high specificity of the hybridization process and excludes any false signals caused by nonspecific absorption. Notably, the biomolecule tagging reaction takes place at the interface between the aqueous phase and SU-8 surface with extreme efficiency. In the absence of any conjugation linkers or mechanical stirring, the one-step reaction completed within an hour. Subsequent rinsing of the silicon substrate conveniently removes any unreacted DNA while retaining all the micropillars on the substrate surface.

Encouraged by the positive results from the biomolecule tagging and hybridization trial on solid substrates, we further explored the ability of fabricated barcodes to support multiplexed biomolecular detection in a suspension assay format. Barcodes of two disparate color arrangements (R–Y–B and Y–G–P), each carrying one unique DNA sequence, are liberated from the substrate and mixed in a 5 µL buffer solution. Cy3-labeled target DNAs are subsequently spiked into the suspension and incubated for 30 min to cater to potential hybridization reactions. After centrifugal washing, aliquots of the barcode suspension were dried on glass slides for luminescence microscopy analysis.

As shown in **Figure 6**, most of the barcodes are monodispersed on the glass slide. The excellent microparticle dispersibility ensures thorough mixing during the hybridization step. A close examination with Cy3 channel (excitation: 535 ± 50 nm, emission: 610 ± 75 nm) reveals that only a portion of the micropillars are stained orange, indicating that hybridization takes place exclusively on these micropillars. To extract the sequence information of hybridized DNA targets, upconversion imaging was performed on this subpopulation of barcodes. All Cy3-stained barcodes carried the color sequence red–yellow–blue (R–Y–B), indicating the existence of a target DNA sequence complementary to the probe strand. Comparatively, the yellow–green–purple (Y–G–P) barcodes in the mixture were tagged with DNA probes noncomplementary to the target DNAs; the hybridization failure between these noncompatible strands renders the barcodes unstained and thus absent under Cy3 channel imaging.

To demonstrate the capability of the barcodes toward a practical intent for multiplexed simultaneous screening of multiple analytes within a single biological mixture, a single suspension assay involving mixed barcodes with differing DNA spike combinations was assessed (Figure S8, Supporting
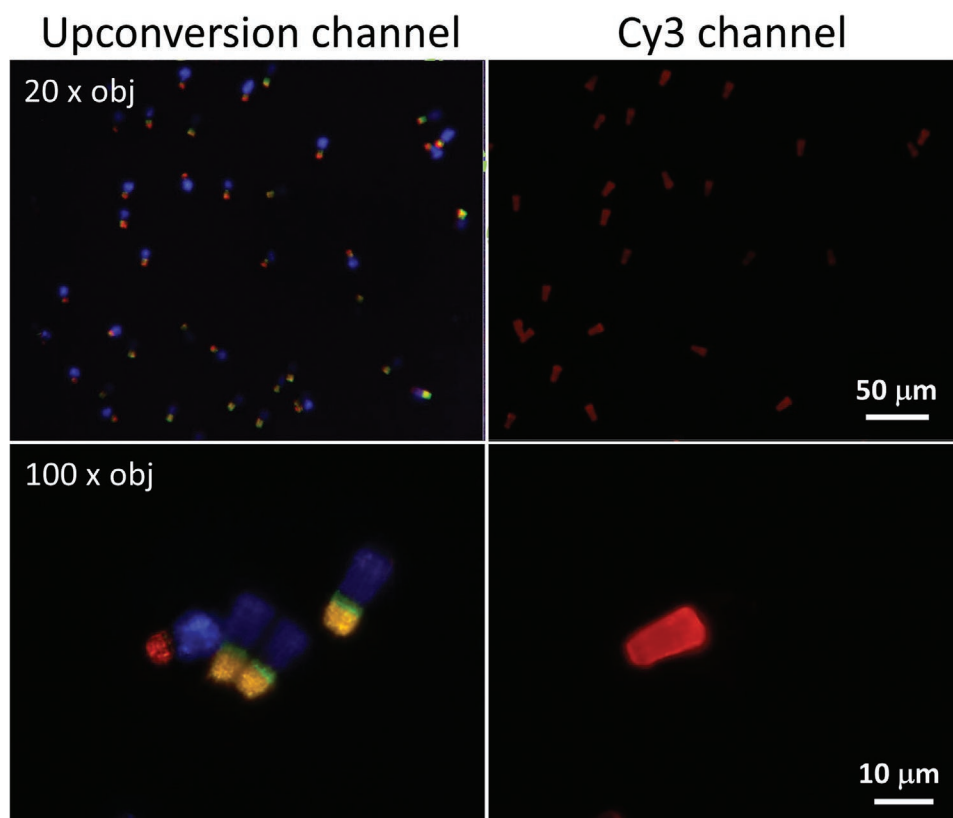
**ADVANCED
SCIENCE NEWS**

www.advancedsciencenews.com

**ADVANCED
OPTICAL
MATERIALS**

www.advopticalmat.de

Figure 6. Proof of concept multiplexed DNA detection using barcode systems. Barcode red–yellow–blue (R–Y–B) carries DNA probe "A" while barcode yellow–green–purple (Y–G–P) carries DNA probe "B." After DNA strands (Cy3 labeled) complementary to probe "A" are spiked to a suspension containing the two types of barcodes, microscopic images reveal that only the R–Y–B barcodes are Cy3 labeled, matching the spiking pattern. This result suggests that the molecular recognition test can be performed on the newly developed barcodes. In the suspension assay, Cy3 channel is used to analyze the concentration of any potentially existing DNA molecules, while the upconversion channel serves to decode the sequence of the DNA.

Information). With probes "A" (R–Y–B) and "B" (Y–G–P) complementary to its respective targets "a" and "b," the permutative assessment further affirmed the exclusiveness of each barcode type toward its intended target. The obtained fluorescence Cy3 and upconverted barcode readings tallied with the tested spiking pattern, suggesting that multiple analytes can be simultaneously detected on this colored-graphical barcode platform. Since decoding and detection are performed on nonoverlapping microscopic channels (upconversion vs downshifting), a low detection limit of 20×10^{-9} M for Cy3-labeled DNA is achieved (Figure S9, Supporting Information). Below 20×10^{-9} M, however, background autofluorescence from SU-8 would contribute to the signal reading. Therefore, the use of low autofluorescence photoresists and redshifted reporting dyes would further assist in the detection of biomarkers that exist in low abundance. The biomolecule-tagged barcodes also enjoy a long shelf life; barcodes preserved in deionized water or phosphate buffer for several months still display capability for sensitive molecule detection. However, we do recommend that the biomolecular tagging be conducted soon after the barcode fabrication to reduce any moisture-induced, epoxy ring-opening reactions. We envision the possibility of pre-loading biomarkers, such as microRNAs and proteins, onto respective microbarcodes to form a stock library, which can be mixed on-site and on-demand to perform customized high throughput molecular profiling.

In summary, we have developed a photolithography-based method for high-speed, low-cost production of encoded microbarcodes. Within the fabricated sub-15 µm micropillars, UCNPs with distinct emission colors are spatially segregated into layered compartments to give a rich library of color combinations for biomolecular labeling in multiplexed molecular detection. The high encoding capacity, cost-effective production, and flexible biomolecular tagging allow barcodes to be tailored to simultaneously identify several specific bioanalytes amidst thousands of biomolecules present within a laboratory or serological sample, marking its potential for large-scale screening in the realm of proteomics, genomics, metabolomics and epidemiological studies.

Experimental Section

Experimental details on nanoparticle synthesis, surface modification, barcode fabrication, SU-8 biomolecule conjugation, and DNA hybridization procedures are available in the Supporting Information.

Supporting Information

Supporting Information is available from the Wiley Online Library or from the author.

[1] a) K. Braeckmans, S. C. De Smedt, M. Leblans, R. Pauwels, J. Demeester, *Nat. Rev. Drug Discovery* **2002**, *1*, 447; b) J. P. Nolan, L. A. Sklar, *Trends Biotechnol.* **2002**, *20*, 9.

[2] a) R. Wilson, A. R. Cossins, D. G. Spiller, *Angew. Chem., Int. Ed.* **2006**, *45*, 6104; b) S. Birtwell, H. Morgan, *Integr. Biol.* **2009**, *1*, 345; c) M. Wang, B. Duong, H. Fenniri, M. Su, *Nanoscale* **2015**, *7*, 11240; d) Y. Leng, K. Sun, X. Chen, W. Li, *Chem. Soc. Rev.* **2015**, *44*, 5552.

[3] a) M. Han, X. Gao, J. Z. Su, S. Nie, *Nat. Biotechnol.* **2001**, *19*, 631; b) S. Fournier-Bidoz, T. L. Jennings, J. M. Klostranec, W. Fung, A. Rhee, D. Li, W. C. Chan, *Angew. Chem., Int. Ed.* **2008**, *47*, 5577; c) S. A. Dunbar, *Clin. Chim. Acta* **2006**, *363*, 71.

[4] K. L. Kellar, J. P. Douglass, *J. Immunol. Methods* **2003**, *279*, 277.

[5] a) M. J. Dejneka, A. Streltsov, S. Pal, A. G. Frutos, C. L. Powell, K. Yost, P. K. Yuen, U. Muller, J. Lahiri, *Proc. Natl. Acad. Sci. USA* **2003**, *100*, 389; b) H. Lee, J. Kim, H. Kim, J. Kim, S. Kwon, *Nat. Mater.* **2010**, *9*, 745; c) S. R. Nicewarner-Peña, R. G. Freeman, B. D. Reiss, L. He, D. J. Peña, I. D. Walton, R. Cromer, C. D. Keating, M. J. Natan, *Science* **2001**, *294*, 137; d) Y. Zhang, L. Huang, X. Liu, *Angew. Chem., Int. Ed.* **2016**, *55*, 5718; e) Y. Zhang, L. Zhang, R. Deng, J. Tian, Y. Zong, D. Jin, X. Liu, *J. Am. Chem. Soc.* **2014**, *136*, 4893; f) D. C. Pregibon, M. Toner, P. S. Doyle, *Science* **2007**, *315*, 1393.

[6] J. Lee, P. W. Bisso, R. L. Srinivas, J. J. Kim, A. J. Swiston, P. S. Doyle, *Nat. Mater.* **2014**, *13*, 524.

[7] a) D. Dendukuri, D. C. Pregibon, J. Collins, T. A. Hatton, P. S. Doyle, *Nat. Mater.* **2006**, *5*, 365; b) J. H. Jang, D. Dendukuri, T. A. Hatton, E. L. Thomas, P. S. Doyle, *Angew. Chem., Int. Ed.* **2007**, *46*, 9027; c) D. Dendukuri, S. S. Gu, D. C. Pregibon, T. A. Hatton, P. S. Doyle, *Lab Chip* **2007**, *7*, 818.

[8] a) G. Chen, H. Qiu, P. N. Prasad, X. Chen, *Chem. Rev.* **2014**, *114*, 5161; b) Y. Liu, Y. Lu, X. Yang, X. Zheng, S. Wen, F. Wang, X. Vidal, J. Zhao, D. Liu, Z. Zhou, C. Ma, J. Zhou, J. A. Piper, P. Xi, D. Jin, *Nature* **2017**, *543*, 229; c) S. Chen, A. Z. Weitemier, X. Zeng, L. He, X. Wang, Y. Tao, A. J. Huang, Y. Hashimotodani, M. Kano, H. Iwasaki, L. K. Parajuli, S. Okabe, D. B. L. Teh, A. H. All, I. Tsutsui-Kimura, K. F. Tanaka, X. Liu, T. J. McHugh, *Science* **2018**, *359*, 679; d) X. Zhu, J. Li, X. Qiu, Y. Liu, W. Feng, F. Li, *Nat. Commun.* **2018**, *9*, 2176; e) X. Li, Z. Guo, T. Zhao, Y. Lu, L. Zhou, D. Zhao, F. Zhang, *Angew. Chem., Int. Ed.* **2016**, *55*, 2464; f) M. Haase, H. Schaefer, *Angew. Chem., Int. Ed. Engl.* **2011**, *50*, 5808; g) Y. Zhong, I. Rostami, Z. Wang, H. Dai, Z. Hu, *Adv. Mater.* **2015**, *27*, 6418; h) X. Ai, Z. Wang, H. Cheong, Y. Wang, R. Zhang, J. Lin, Y. Zheng, M. Gao, B. Xing, *Nat. Commun.* **2019**, *10*, 1087; i) B. Ding, S. Shao, C. Yu, B. Teng, M. Wang, Z. Cheng, K. L. Wong, P. Ma, J. Lin, *Adv. Mater.* **2018**, *30*, 1802479.

[9] a) F. Zhang, Q. Shi, Y. Zhang, Y. Shi, K. Ding, D. Zhao, G. D. Stucky, *Adv. Mater.* **2011**, *23*, 3775; b) Y. Fan, P. Wang, Y. Lu, R. Wang, L. Zhou, X. Zheng, X. Li, J. A. Piper, F. Zhang, *Nat. Nanotechnol.* **2018**, *13*, 941; c) L. Zhou, Y. Fan, R. Wang, X. Li, L. Fan, F. Zhang, *Angew. Chem., Int. Ed.* **2018**, *57*, 12824; d) H. Zhang, Y. Fan, P. Pei, C. Sun, L. Lu, F. Zhang, *Angew. Chem., Int. Ed.* **2019**, *58*, 10153; e) H. H. Gorris, O. S. Wolfbeis, *Angew. Chem., Int. Ed.* **2013**, *52*, 3584.

[10] a) L. Zhou, R. Wang, C. Yao, X. Li, C. Wang, X. Zhang, C. Xu, A. Zeng, D. Zhao, F. Zhang, *Nat. Commun.* **2015**, *6*, 6938; b) X. Qin, J. Xu, Y. Wu, X. Liu, *ACS Cent. Sci.* **2019**, *5*, 29; c) F. Wang, R. Deng, J. Wang, Q. Wang, Y. Han, H. Zhu, X. Chen, X. Liu, *Nat. Mater.* **2011**, *10*, 968.

[11] a) J. Liu, L. Pan, C. Shang, B. Lu, R. Wu, Y. Feng, W. Chen, R. Zhang, J. Bu, Z. Xiong, W. Bu, J. Du, J. Shi, *Sci. Adv.* **2020**, *6*, eaax9757; b) Z. Di, B. Liu, J. Zhao, Z. Gu, Y. Zhao, L. Li, *Sci. Adv.* **2020**, *6*, eaba9381; c) S. Wen, J. Zhou, K. Zheng, A. Bednarkiewicz, X. Liu, D. Jin, *Nat. Commun.* **2018**, *9*, 2415; d) A. H. All, X. Zeng, D. B. L. Teh, Z. Yi, A. Prasad, T. Ishizuka, N. Thakor, Y. Hiromu, X. Liu, *Adv. Mater.* **2019**, *31*, 1803474; e) X. Zeng, S. Chen, A. Weitemier, S. Han, A. Blasiak, A. Prasad, K. Zheng, Z. Yi, B. Luo, I. H. Yang, N. Thakor, C. Chai, K. L. Lim, T. J. McHugh, A. H. All, X. Liu, *Angew. Chem., Int. Ed.* **2019**, *58*, 9262.

[12] a) R. Marie, S. Schmid, A. Johansson, L. Ejsing, M. Nordström, D. Häfliger, C. B. V. Christensen, A. Boisen, M. Dufva, *Biosens. Bioelectron.* **2006**, *21*, 1327; b) G. Blagoi, S. Keller, A. Johansson, A. Boisen, M. Dufva, *Appl. Surf. Sci.* **2008**, *255*, 2896.